ELSEVIER

NeuroImage

www.elsevier.com/locate/ynimg
NeuroImage 22 (2004) 1302–1314

Diffusion tensor imaging: serial quantitation of white matter tract maturity in premature newborns ☆

Savannah C. Partridge,[a] Pratik Mukherjee,[a] Roland G. Henry,[a] Steven P. Miller,[b,c] Jeffrey I. Berman,[a] Hua Jin,[a] Ying Lu,[a] Orit A. Glenn,[a] Donna M. Ferriero,[b,c] A. James Barkovich,[a,b,c] and Daniel B. Vigneron[a,*]

[a] *Department of Radiology, University of California, San Francisco, San Francisco, CA 94143, USA*
[b] *Department of Neurology, University of California, San Francisco, San Francisco, CA 94143, USA*
[c] *Department of Pediatrics, University of California, San Francisco, San Francisco, CA 94143, USA*

Received 11 December 2003; revised 25 February 2004; accepted 26 February 2004

Available online 7 May 2004

Magnetic resonance diffusion tensor imaging (DTI) enables the discrimination of white matter pathways before myelination is evident histologically or on conventional MRI. In this investigation, 14 premature neonates with no evidence of white matter abnormalities by conventional MRI were studied with DTI. A custom MR-compatible incubator with a novel high sensitivity neonatal head coil and improved acquisition and processing techniques were employed to increase image quality and spatial resolution. The technical improvements enabled tract-specific quantitative characterization of maturing white matter, including several association tracts and subcortical projection tracts not previously investigated in neonates by MR. Significant differences were identified between white matter pathways, with earlier maturing commissural tracts of the corpus callosum, and deep projection tracts of the cerebral peduncle and internal capsule exhibiting lower mean diffusivity (D_{av}) and higher fractional anisotropy (FA) than later maturing subcortical projection and association pathways. Maturational changes in white matter tracts included reductions in D_{av} and increases in FA with age due primarily to decreases in the two minor diffusion eigenvalues (λ_2 and λ_3). This work contributes to the understanding of normal white matter development in the preterm neonatal brain, an important step toward the use of DTI for the improved evaluation and treatment of white matter injury of prematurity.

Keywords: Diffusion; White matter; Maturity

Introduction

Noninvasive imaging of neonates born prematurely is of great scientific interest because it offers a unique window into early human cerebral development. The axonal connectivity between brain regions is established during this preterm period, providing an opportunity to study the formation of white matter pathways. Moreover, the white matter tracts in the cerebral hemispheres of the premature brain are unmyelinated, except for a few early-maturing pathways such as the pyramidal tract as the baby approaches term-equivalent age (Kinney et al., 1988, 1994). The maturational processes associated with neuronal development and "premyelination" (Wimberger et al., 1995), as well as the onset of myelination can be evaluated quantitatively with magnetic resonance diffusion tensor imaging (DTI) which is sensitive to changes in tissue microstructure.

Understanding early human brain development is also of great clinical importance because a multitude of neurological and psychiatric disorders are known to have a neurodevelopmental basis. Some of these, such as autism and attention deficit hyperactivity disorder, are very prevalent and are diagnosed with increasing frequency (Fombonne, 2003; Spencer et al., 2002). Furthermore, premature birth itself is an increasingly common public health problem. The rate of prematurity exceeded 11% of all live births in the United States in 2000 (Martin et al., 2002), and its incidence continues to rise. Premature infants are vulnerable to a host of medical problems, many of which involve the central nervous system. Associated neurologic deficits include spastic diplegia, visual impairment, cognitive deficiencies, and behavioral disorders (Bhutta et al., 2002; Hack et al., 2002; Wood et al., 2000). These poor clinical outcomes are thought to be related to injury of the white matter (Volpe, 2001). The early detection of abnormal white matter maturation in preterm neonates may impact their clinical care. Cranial sonography, the primary method of screening premature newborns (Ment et al., 2002), is not nearly as sensitive as MR imaging to white matter injury (Inder et al., 2003; Miller et al., 2003). However, conventional T1- and T2-weighted MR imaging sequences are also limited in the evaluation of the

☆ This work was supported by grants from the National Institutes of Health (RO1 NS40117, R21 NS40382, RR01271, and P50 NS35902).

* Corresponding author. Magnetic Resonance Science Center, Department of Radiology, University of California, San Francisco, Box 1290, 1 Irving Street, Suite AC-109, San Francisco, CA 94143-1290. Fax: +1-415-476-8809.

E-mail address: daniel.vigneron@radiology.ucsf.edu (D.B. Vigneron).

Available online on ScienceDirect (www.sciencedirect.com.)

1053-8119/$ - see front matter © 2004 Elsevier Inc. All rights reserved.
doi:10.1016/j.neuroimage.2004.02.038

preterm brain, as they are able to detect only macroscopic injury and do not allow visualization of specific white matter tracts before the onset of myelination.

Diffusion-weighted MR imaging enables the visualization and quantitative characterization of white matter pathways before myelination is evident histologically or on conventional MRI (Wimberger et al., 1995). Prior studies have demonstrated the ability of diffusion tensor imaging (DTI) to identify maturational trends reflecting microstructural changes in white matter and gray matter of the developing brain (Boujraf et al., 2002; Huppi et al., 1998; Miller et al., 2002; Mukherjee et al., 2001, 2002; Neil et al., 1998). The directionally averaged magnitude of water diffusion, D_{av}, decreases with increasing age during preterm development. Structural and physiological changes in maturing axons, even before myelination, cause water diffusion to become more reduced in directions orthogonal to the long axis of the white matter fibers than parallel to the fibers (Prayer et al., 2001; Wimberger et al., 1995). This diffusion anisotropy is the basis for discriminating white matter with DTI. Anisotropy increases in white matter with increasing gestational age during preterm development. However, in premature newborns with white matter injury, these maturational trends in D_{av} and anisotropy may be diminished or even reversed (Arzoumanian et al., 2003; Huppi et al., 2001; Miller et al., 2002).

The very low anisotropy of premyelinating white matter and the very small size of white matter tracts in premature newborns present serious technical challenges for DTI due to signal-to-noise ratio (SNR) and spatial resolution constraints. Until now, these considerations have limited the measurement of diffusion tensor parameters in the developing preterm brain to the large, early maturing commissural pathways of the corpus callosum and the projection pathways of the pyramidal tract in the internal capsule (Huppi et al., 1998; Neil et al., 1998). Additionally, prior DTI studies of white matter maturation in preterm neonates have primarily relied on cross-sectional designs. This approach is limited by uncertainty in estimates of corrected gestational age and by large variations among preterm neonates in their gestational age at birth (Miller et al., 2002). Both these factors may potentially affect cross-sectional data on white matter development, the latter because ex utero brain maturation may proceed more slowly than in utero development (Huppi et al., 1998).

A recently developed MR-compatible incubator with a specialized high-sensitivity neonatal head coil (Dumoulin et al., 2002) and improved acquisition and processing techniques now allow us to perform DTI at higher spatial resolution and higher SNR than in previous studies. In this investigation, serial DTI examinations in premature newborns were employed to quantitatively characterize development in smaller white matter pathways than had previously been possible, including several cortical association tracts. The serial examinations permit the longitudinal assessment of brain development in individual infants, and are not subject to the potentially confounding effects of estimating gestational age and of variation in gestational age at birth. New analysis software was also developed for directional color encoding of fiber orientation in white matter tracts, to facilitate identification of specific axonal pathways for quantitation. In addition to the D_{av} and anisotropy information provided in previous DTI studies of the premature brain (Huppi et al., 1998, 2001; Miller et al., 2002; Neil et al., 1998), the three eigenvalues of the diffusion tensor were measured in this study to provide a more direct assessment of the directional diffusion changes associated with white matter development.

Materials and methods

Subjects

The patients eligible for this study were neonates born at gestational ages of 24 to 36 weeks with no evidence of white matter injury on conventional MR imaging. Gestational age (GA) was calculated based on the mother's last menstrual period or estimates from early sonography (<24 weeks). Infants were excluded from the study if there was evidence of greater than Grade 1 hemorrhage (i.e., small intraventricular bleed confined to the subependymal region), congenital infection, brain malformation, or a multiple congenital anomaly syndrome. Clinical data such as birth weight, sex, gestational age at birth, and gestational age at the time of imaging were recorded. An institutional review board approved the study protocol, and informed parental consent was obtained for each subject.

Over the 28-month duration of the study (between November 8, 2001 and March 5, 2003), 50 premature neonates were imaged with MRI at our institution and 15 of them met the inclusion criteria. Of 24 MRI exams acquired in these 15 patients, two exams were excluded due to motion artifacts that substantially degraded the DTI acquisition. As a result, 14 preterm newborns were included in the study. Gestational ages at birth were between 25 and 34 weeks (median, 29 weeks), and birth weights ranged from 635 to 2145 g (mean, 1277 g). The infants were first imaged between 28 and 39 weeks GA (median, 33 weeks), and eight of the infants were studied serially and received their second MR exam at or near term age or just before discharge from the hospital. The median time between serial MR exams was 5 weeks (range, 2–7 weeks), and the ages of the infants at their second scans were between 35 and 43 weeks (median, 37.5 weeks).

MR acquisition

Technical requirements for optimal DTI data acquisition in the neonatal brains included full brain coverage with no gap between slices, high spatial resolution, and minimizing motion artifact. These requirements were primarily met by newly developed imaging hardware. The custom MR-compatible incubator with a specialized neonatal head coil (Dumoulin et al., 2002) was used for all image acquisition in this study. The incubator provides a warm, quiet, and well-monitored environment, which allows imaging to be performed earlier after birth. The babies were transferred and acclimated to the MR-compatible incubator in the neonatal intensive care unit and positioned in the center of the neonatal head coil using custom padding. The use of cotton ear muffs, comfortable contoured padding, warm environment, double-walled construction, and acoustic and vibration damping all tend to facilitate undisturbed sleep and/or calm resting during the MR scans, permitting non-sedated studies with negligible motion artifacts. The system design also includes a custom-built birdcage radiofrequency coil with increased performance over standard head coils for imaging the small neonates. The coil incorporates a recessed ring design for improved accessibility with a much narrower diameter around the neonatal head, providing higher signal-to-noise (SNR) images than conventional head coils. In a limited number of comparisons conducted previously for similarly sized neonates of similar gestational ages, improvements in SNR of the specialized coil were found to range from 40% to 70% over a standard head coil, depending on the subject.

All imaging was performed on a 1.5-T GE EchoSpeed scanner (GE Medical Systems, Milwaukee, WI) using the new MR-compatible incubator and neonatal head coil. The diffusion tensor imaging data were acquired in 4.8 min using a multi-repetition, single-shot echo planar sequence with six gradient directions, b = 0 and 600 s/mm^2, TR = 7 s, TE = 99.5 ms, three repetitions, FOV = 36 × 18 cm, matrix = 256 × 128, slice thickness = 3 mm with no gap, 167 kHz readout band width, and no ramp sampling. The resulting in-plane resolution was 1.4 mm. The number of slices acquired in each exam varied with infant head size, but typically 22 interleaved axial slices were required for full brain coverage.

Diffusion tensor post-processing

Diffusion-weighted images were transferred off-line for processing, and were first aligned using a 2D 10th order nonlinear (858 parameter) spatial transformation algorithm (AIR 5.1, Woods et al., 1998a,b). The 2D warping registration was used to correct for inter-slice patient motion and variations in EPI image distortion due to eddy currents induced by the diffusion gradients. The T2-weighted (b = 0 s/mm^2) EPI images were used as reference for registration of the corresponding b = 600 s/mm^2 DTI images.

Using software developed in-house, parametric maps were then generated for the six rotationally invariant DTI parameters: the directionally averaged diffusion coefficient (D_{av}), fractional anisotropy (FA), relative anisotropy (RA), and the maximum, intermediate, and minimum eigenvalues (λ_1, λ_2, and λ_3, respectively), and their associated eigenvectors, based on the methods proposed by Basser and Pierpaoli (1996). The eigenvalues (or principal diffusivities) of the diffusion tensor characterize the magnitude or rate of water diffusion along each of the three principal axes of the diffusion tensor ellipsoid, given in mm^2/s. The direction of each of these three principal axes in 3D space is given by the eigenvectors. The one associated with the maximum eigenvalue, the principal eigenvector, corresponds to the fiber tract orientation in coherently organized white matter fiber bundles. D_{av}, the mean diffusivity (in mm^2/s), was calculated using the formula

$$D_{av} = \frac{\lambda_1 + \lambda_2 + \lambda_3}{3}. \quad (1)$$

Fractional anisotropy (FA), a dimensionless measure of anisotropy, expresses the fraction of the magnitude of the diffusion tensor attributable to anisotropic diffusion and was calculated by

$$\mathrm{FA} = \sqrt{\frac{3}{2}} \frac{\sqrt{\sum_{i=1}^{3} (\lambda_i - D_{av})^2}}{\sqrt{\lambda_1^2 + \lambda_2^2 + \lambda_3^2}} = \frac{\sqrt{(\lambda_1 - \lambda_2)^2 + (\lambda_2 - \lambda_3)^2 + (\lambda_3 - \lambda_1)^2}}{\sqrt{2}\sqrt{\lambda_1^2 + \lambda_2^2 + \lambda_3^2}}. \quad (2)$$

For isotropic diffusion ($\lambda_1 = \lambda_2 = \lambda_3$), FA is zero, and in the case where there is a strongly preferred direction of diffusion ($\lambda_1 >> \lambda_2 = \lambda_3$), FA approaches one.

Prior diffusion tensor imaging studies have used other indices to describe the degree of preferred direction of water diffusion, such as relative anisotropy (RA). RA expresses the ratio of anisotropic to isotropic diffusion, and is defined as the standard deviation of the eigenvalues of the diffusion tensor divided by the mean, D_{av}, given by

$$\mathrm{RA} = \frac{\sqrt{\sum_{i=1}^{3} (\lambda_i - D_{av})^2}}{\sqrt{3} D_{av}} = \frac{\sqrt{(\lambda_1 - \lambda_2)^2 + (\lambda_2 - \lambda_3)^2 + (\lambda_3 - \lambda_1)^2}}{\lambda_1 + \lambda_2 + \lambda_3} \quad (3)$$

RA, also a dimensionless measure, is zero for isotropic diffusion and approaches $\sqrt{2}$ in the case of high anisotropy. Simulations assuming cylindrical symmetry have shown that RA is linear over the complete range of fiber anisotropy values, whereas FA is nonlinear, with higher sensitivity at lower anisotropy values (Ulug and van Zijl, 1999). For this reason, it was felt that the expansive nonlinearity in FA at low anisotropy values would better distinguish between regions of low anisotropy in the neonatal brain. Nevertheless, RA was also calculated and included in the analysis for comparison.

Color directional anisotropy maps

Color overlay representation of the principal eigenvector data on the anisotropy maps was performed to facilitate identification of specific tracts by indicating fiber direction by color. The principal eigenvector was mapped to an orthogonal coordinate system and represented by color encoding of the anisotropy maps (Pajevic and Pierpaoli, 1999). In this study, color representation was achieved by overlaying three directional anisotropy maps, each weighted by the component of the principal eigenvector in a particular orthogonal direction, and using the alpha channel of the 24-bit graphics display to blend the images. The brightness of the color overlay image was scaled by the FA to avoid representation of voxels with low anisotropy, where the principal eigenvector is not correlated with fiber direction. The color representation of fiber orientation was based on the assumption of both mirror and rotational symmetry, using the absolute value of the principal eigenvector components. The color convention used was based on the absolute value scheme reported by Pajevic and Pierpaoli (1999), with red representing right–left (R/L), green representing anteroposterior (A/P), and blue representing superoinferior (S/I) anatomical directions.

The translucency of each overlay image was a function of the component of the principal eigenvector in each of the three orthogonal directions. Using the alpha channel, voxels in the foreground image with a value of zero were set to totally transparent and did not contribute to the displayed image, while non-zero voxels were semi-transparent with translucency proportional to their values. The highest valued voxels were set to totally opaque on the display. In this way, when displaying the green A/P directional map, for example, voxels with principal eigenvectors fully in the A/P direction (zero components in the R/L or S/I directions) were opaque green, and those with small components in the A/P direction were mostly transparent and contributed little green to the color of the voxels in the resulting image (with color instead coming from the red R/L and/or blue S/I maps). Slider bars were incorporated to allow the user to change the maximum opacity weighting for each color interactively to allow the background image to show through, useful for displaying color maps

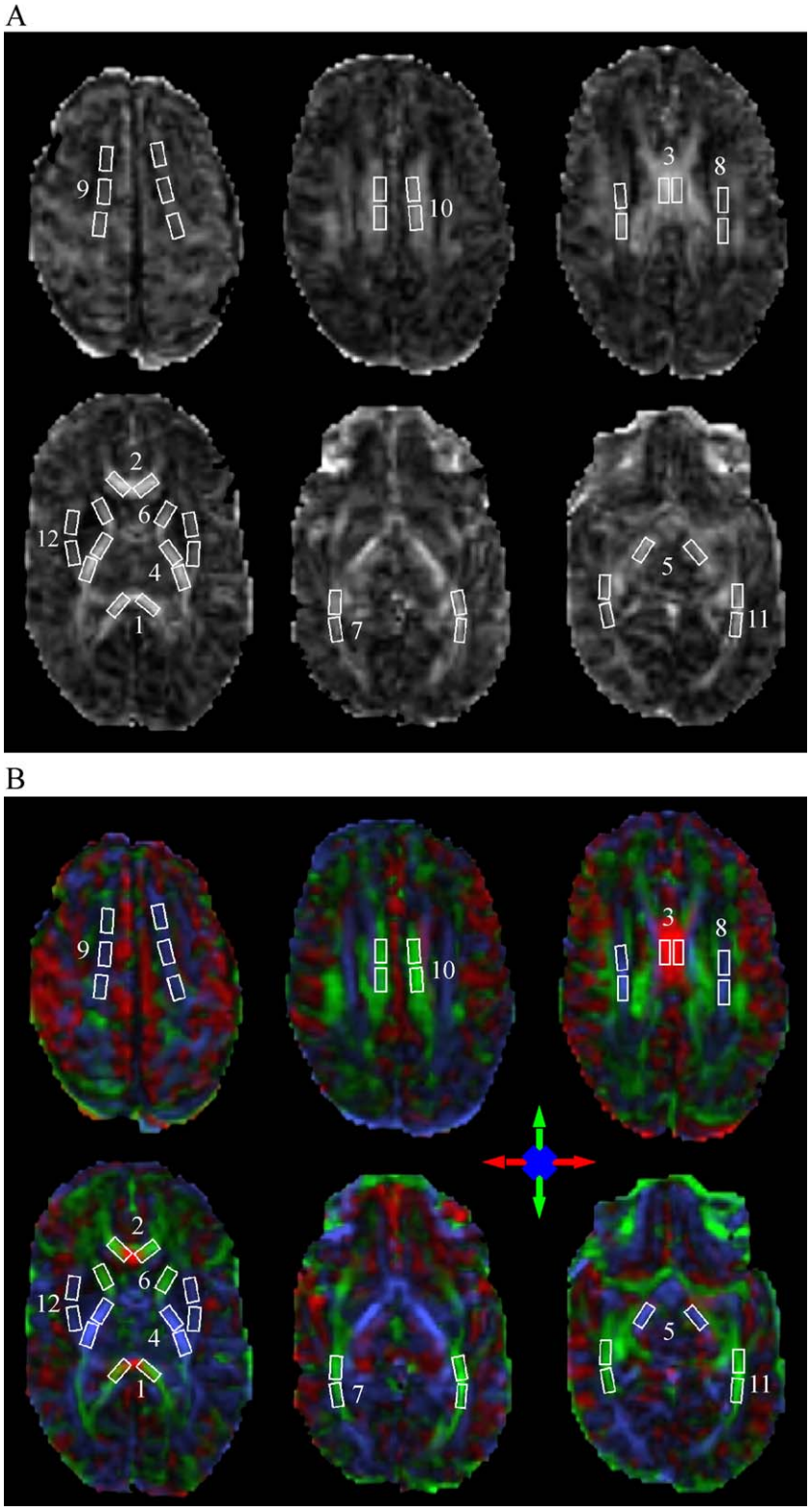

Fig. 1. Representative ROI placement for white matter tracts measured in the study, shown on both grayscale FA maps (a) and directionally encoded anisotropy color maps (b) from a premature newborn scanned at 35 weeks gestational age. The 12 white matter structures measured in the study were the (1) splenium, (2) genu, and (3) body of the corpus callosum, (4) posterior limb of the internal capsule, (5) cerebral peduncle, (6) anterior limb of the internal capsule, (7) optic radiation, (8) low centrum semiovale (at the level of the body of the corpus callosum), (9) high centrum semiovale (above the lateral ventricles), (10) cingulum, (11) inferior longitudinal fasciculus, and (12) external/extreme capsule.

overlaid on a grayscale anatomic image for instance. In addition, slider bars allowed the user to threshold color overlays based on the magnitude of underlying anisotropy to represent color directional information only on voxels above a particular anisotropy threshold. This enabled quick graphic comparison of anisotropy values in different structures in a more straightforward way than interpretations based on perceived differences in brightness, and was especially useful for comparing structures contained in different slice locations.

White matter DTI measurements

As premature newborns are at risk for motor, visual, and cognitive defects, we focused on multiple tracts involved in these processes. The tracts selected for quantitation in the study included *commissural tracts* of the corpus callosum at its (1) splenium, (2) genu, and (3) body; *projection tracts* measured at the (4) posterior limb of the internal capsule, (5) cerebral peduncle, (6) anterior limb of the internal capsule, (7) optic radiation, (8) low centrum semiovale (below the roof of the lateral ventricles, at the level of the body of the corpus callosum) and (9) high centrum semiovale (above the lateral ventricles); and *association tracts* of the (10) cingulum, (11) inferior longitudinal fasciculus (ILF), and (12) external/extreme capsule. The motor fibers of the pyramidal tract are known to run through the cerebral peduncle, posterior limb of the internal capsule, and centrum semiovale. The optic radiation and inferior longitudinal fasciculus are involved with vision and visual associative functions, respectively. Other white matter structures contain association tracts involved in cognitive tasks such as conflict monitoring (cingulum) or language function (external/extreme capsules), while the commissural fibers of the corpus callosum mediate the interhemispheric transfer of cognitive information.

DTI measurements were taken from multiple regions of interest (ROIs) positioned bilaterally within individual white matter tracts defined on the color directional anisotropy maps by an experienced neuroradiologist. ROI placement was further validated against corresponding D_{av} maps and T2-weighted (b = 0 s/mm^2) images to exclude any adjacent ventricular cerebrospinal fluid from the measurements. Fig. 1 illustrates typical ROIs for the 12 structures, overlaid on both the grayscale FA maps (Fig 1a) and directionally encoded color FA maps (Fig. 1b).

Statistical analysis

For each subject, median ROI values were measured for all 12 regions in each hemisphere. Statistical differences between right and left ROIs were assessed with a two-tailed paired Student's t test.

Differences in DTI values between structures (independent of age)

Mixed random-effects models (Laird and Ware, 1982) were employed to assess the differences in diffusion parameters between different tracts. The analyses were performed controlling for age at time of scan. All 14 infants were included in the analysis, and repeated measures from the same infant at different ages across serial examinations were also controlled for in the mixed random-effects model. Significance of the difference between structures was calculated based on analysis of ranks of the diffusion parameters.

Age-dependent maturational changes

Maturational changes in white matter DTI parameters were quantified in the eight infants studied serially, and the percent change per week of gestational age was used to compare maturation rates between different DTI parameters and between different white matter tracts. This investigation required two different types of statistical analyses. First, it was necessary to determine whether there were significant developmental changes in diffusion parameters between two serial scans in the same individual. This analysis was restricted to each individual tract. The median changes of diffusion parameters and the corresponding P values for differences from zero based on the Wilcoxon signed rank test (Maritz, 1985) were determined for each structure for robust estimation of the changes. Next, mixed random-effects models were employed to assess the differences in maturational rates between different tracts. The analyses were performed controlling for the fixed effect of age at scan and structure of interest. In the mixed effects model analyses, it was first determined if there existed statistically significant differences in change of DTI parameters with subject age between different structures of interest, at a significance level of $P < 0.05$. If there was a significant difference between structures, the least squares means of the changes as well as the pairwise differences between structures were calculated. P values were calculated based on analysis of ranks of the diffusion parameters, and P values for pairwise differences were corrected for multiple comparisons using Tukey–Kramer adjustment (Hochberg and Tamhane, 1987). If no overall significant difference was found in the mixed random-effects model analyses, it was inferred that there were no significant differences in change of parameters between different tracts.

Results

The new hardware and software techniques substantially improved DTI SNR by 40% to 70% over prior exams of premature infants employing a standard adult head coil (Miller et al., 2002). The improvement in spatial resolution afforded by this increase in SNR allowed better visualization of small, unmyelinated axonal tracts. Fig. 2a illustrates DTI parameter maps from serial exams of an infant born at 33 weeks gestational age. Many white matter tracts were measurable at the earlier gestational ages, and notable increases in subcortical tract development were visible at term-equivalent age, as also shown in the directionally encoded color FA images of Fig. 2b.

Comparison of DTI values between the left and right hemispheres in each subject demonstrated no statistically significant differences based on a two-tailed paired Student's t test (at a significance level of $P < 0.05$). Therefore, the values obtained from the left and right hemispheres were averaged to obtain the mean D_{av}, FA, RA, λ_1, λ_2, and λ_3 values for each structure.

Differences in DTI values between structures

In the 14 premature neonates, statistically significant ($P < 0.05$) variation in DTI values was observed between white matter structures. Least squares means and standard errors of DTI values for each structure are given in Table 1. FA was highest in the commissural tracts of the corpus callosum, especially the splenium

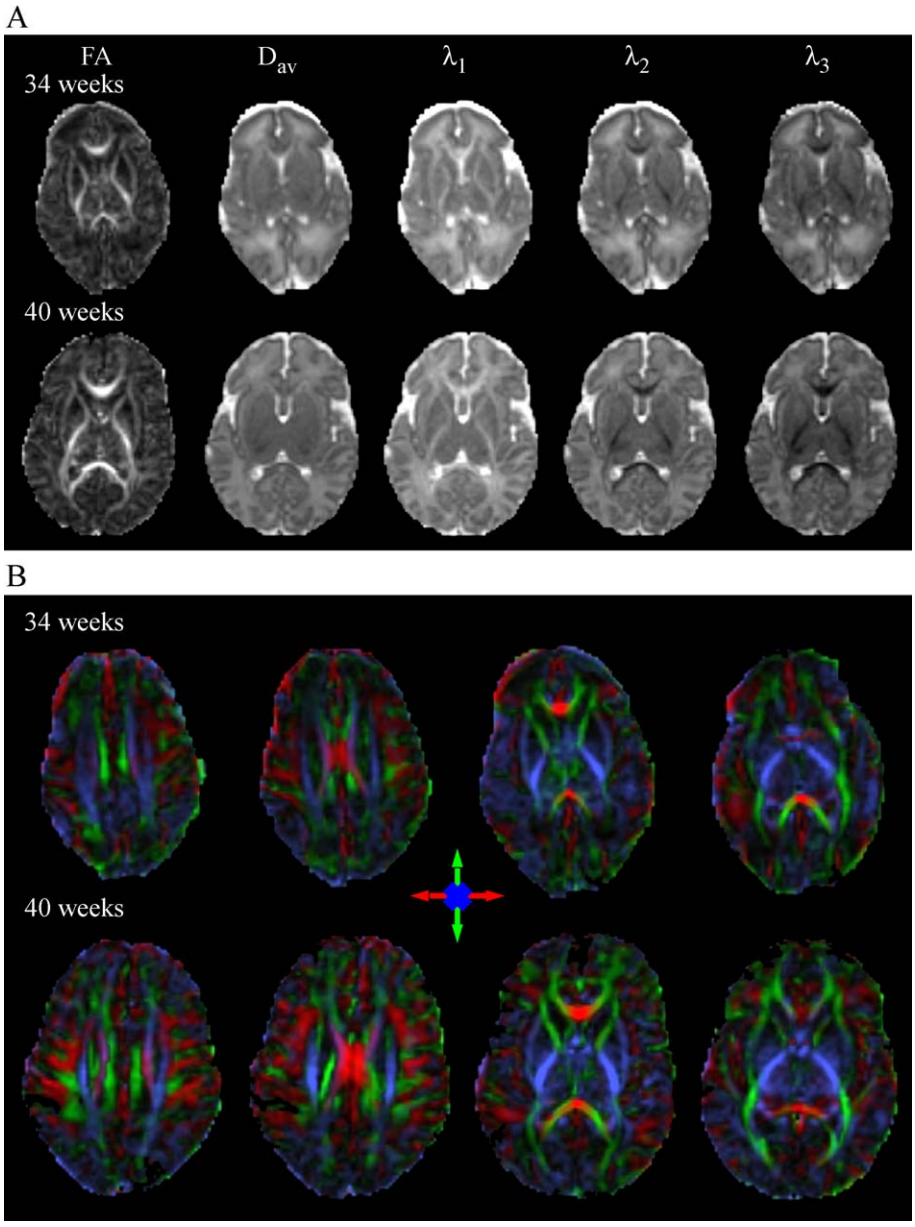

Fig. 2. Images obtained from an infant born at 33 weeks and studied serially at 34 weeks and 40 weeks gestational age. Shown are representative DTI parametric maps (a) for (left to right) FA, D_{av}, λ_1, λ_2, and λ_3 at a single slice location, and directionally encoded anisotropy color maps from four slice locations (b). For both illustrations (a) and (b), the top row shows images acquired at 34 weeks and the bottom row shows images at 40 weeks gestational age. Image scaling and window/levels are proportional for the two ages. Notable increases in subcortical tract development were visible between the earlier and later scans, particularly evident in the directionally encoded color FA images at multiple slice locations (b).

and the genu, followed by the deep projection tracts of the internal capsule and cerebral peduncle. FA was lowest in the association tracts and in the subcortical projection tracts of the centrum semiovale. The commissural tracts of the corpus callosum had the highest values of the major eigenvalue λ_1, with the splenium, genu, and body being the only white matter pathways with median λ_1 values exceeding 2.0×10^{-3} mm^2/s. In contrast, D_{av} was lowest in the deep projection tracts of the cerebral peduncle and the internal capsule, with values less than 1.1×10^{-3} mm^2/s, whereas higher D_{av} values were identified in commissural, subcortical projection (centrum semiovale), and association pathways. The minor eigenvalues, λ_2 and λ_3, showed the same general pattern as D_{av}, with the lowest values in the cerebral peduncle and the posterior limb of the internal capsule.

Table 2 gives the results of pairwise comparisons between the different tracts and illustrates the significant differences in DTI parameters between regions for the age range investigated. As can be observed in the table, the sensitivity for differentiating between structures varied for the different DTI parameters. FA was the most sensitive, and significantly discriminated between 52 pairs of structures. RA discriminated 50 pairs, followed by λ_2 (47 pairs), λ_1 and λ_3 (46 pairs each), and lastly D_{av}, which was the least sensitive parameter and discriminated between 45 pairs of structures.

Table 1
DTI Parameters for 12 white matter structures (least squares means, standard errors)

	Commissural tracts			Projection tracts						Association tracts		
	CC Splen	CC Genu	CC Body	Post L IC	Cereb Ped	Ant L IC	Optic Rad	Low CSem	High CSem	Cingulum	ILF	Ext Cap
FA	0.47	0.43	0.34	0.41	0.35	0.29	0.28	0.24	0.20	0.25	0.24	0.22
	0.010	0.010	0.010	0.010	0.011	0.010	0.010	0.010	0.010	0.010	0.011	0.010
RA	0.41	0.38	0.29	0.35	0.30	0.24	0.24	0.20	0.17	0.21	0.20	0.18
	0.010	0.010	0.010	0.010	0.010	0.010	0.010	0.010	0.010	0.010	0.010	0.010
D_{av}	1.33	1.40	1.52	1.17	1.19	1.30	1.47	1.48	1.57	1.41	1.54	1.36
	0.022	0.022	0.022	0.022	0.023	0.022	0.022	0.022	0.022	0.022	0.024	0.022
λ_1	2.11	2.10	2.11	1.75	1.69	1.72	1.92	1.85	1.88	1.77	1.93	1.66
	0.025	0.025	0.025	0.025	0.025	0.025	0.025	0.025	0.025	0.025	0.026	0.025
λ_2	1.12	1.24	1.39	1.00	1.10	1.17	1.39	1.40	1.56	1.35	1.49	1.34
	0.026	0.026	0.026	0.026	0.027	0.026	0.026	0.026	0.026	0.026	0.028	0.026
λ_3	0.84	0.91	1.10	0.81	0.83	1.01	1.11	1.20	1.28	1.10	1.22	1.09
	0.026	0.026	0.026	0.026	0.027	0.026	0.026	0.026	0.026	0.026	0.028	0.026

D_{av}, λ_1, λ_2, λ_3 in units ($\times 10^{-3}$ mm^2/s). Abbreviations: CC = corpus callosum, Splen = splenium, IC = internal capsule, Post L = posterior limb, Ant L = anterior limb, Cereb Ped = cerebral peduncle, CSem = centrum semiovale, Rad = radiation, ILF = inferior longitudinal fasciculus, Ext Cap = external/extreme capsule.

Table 2
Significant DTI differences between structures ($P < 0.05$)

	Commissural tracts			Projection tracts						Association tracts		
	CC Splenium	CC Genu	CC Body	Post Limb IC	Cereb Peduncle	Ant Limb IC	Optic Radiation	Low CSemi	High CS	Cingulum	Inferior LF	Ext Cap
CC splenium		λ**2**	**D**$_{av}$ FA, RA λ**2,3**	D_{av} FA, RA λ1,2	D_{av} FA, RA λ1	FA, RA λ1,**3**	**D**$_{av}$ FA, RA λ1,**2,3**	**D**$_{av}$ FA, RA λ1,**2,3**	**D**$_{av}$ FA, RA λ1,**2,3**	FA, RA λ1,**2,3**	**D**$_{av}$ FA, RA λ1,**2,3**	FA, RA λ1,**2,3**
CC genu			**D**$_{av}$ FA, RA λ**2,3**	D_{av} λ1,2,3	D_{av} FA, RA λ1,2	D_{av} FA, RA λ1,**3**	FA, RA λ1,**2,3**	FA, RA λ1,**2,3**	**D**$_{av}$ FA, RA λ1,**2,3**	FA, RA λ1,**2,3**	**D**$_{av}$ FA, RA λ1,**2,3**	FA, RA λ1,**2,3**
CC body				D_{av} **FA**, **RA** λ1,2,3	D_{av} λ1,2,3	D_{av} FA, RA λ1,2	FA, RA λ1	FA, RA λ1	FA, RA λ1,**2,3**	D_{av} FA, RA λ1	FA, RA λ1,**3**	D_{av} FA, RA λ1
Posterior limb IC					FA, RA	**D**$_{av}$ FA, RA λ**2,3**	**D**$_{av}$ FA, RA λ**1,2,3**	**D**$_{av}$ FA, RA λ**1,2,3**	**D**$_{av}$ FA, RA λ**1,2,3**	**D**$_{av}$ FA, RA λ**2,3**	**D**$_{av}$ FA, RA λ**1,2,3**	**D**$_{av}$ FA, RA λ**2,3**
Cerebral peduncle						**D**$_{av}$ FA, RA λ**3**	**D**$_{av}$ FA, RA λ**1,2,3**	**D**$_{av}$ FA, RA λ**1,2,3**	**D**$_{av}$ FA, RA λ**1,2,3**	**D**$_{av}$ FA, RA λ**2,3**	**D**$_{av}$ FA, RA λ**1,2,3**	**D**$_{av}$ FA, RA λ**2,3**
Anterior limb IC							**D**$_{av}$ λ**1,2,3**	**D**$_{av}$ FA, RA λ**1,2,3**	**D**$_{av}$ FA, RA λ**1,2,3**	**D**$_{av}$ FA λ**2**	**D**$_{av}$ FA, RA λ**1,2,3**	FA, RA λ**2**
Optic radiation								FA, RA	**D**$_{av}$ FA, RA λ**2,3**	λ1	. . .	D_{av} FA, RA λ1
Low centrum semiovale									λ**2**	λ3	. . .	D_{av} λ1,3
High centrum semiovale										D_{av} **FA**, **RA** λ2,3	**FA**	D_{av} λ1,2,3
Cingulum											**D**$_{av}$ λ**1,2,3**	λ1
Inferior LF												D_{av} λ1,2,3

Significant difference defined as $P < 0.05$, determined by mixed random-effects modeling and signed rank analysis. Bold indicates column variable is higher valued than row variable. Abbreviations: D_{av} = mean diffusivity, FA = fractional anisotropy, CC = corpus callosum, IC = internal capsule, Cereb = cerebral, CSemi = centrum semiovale, LF = longitudinal fasciculus. Ext = external/extreme.

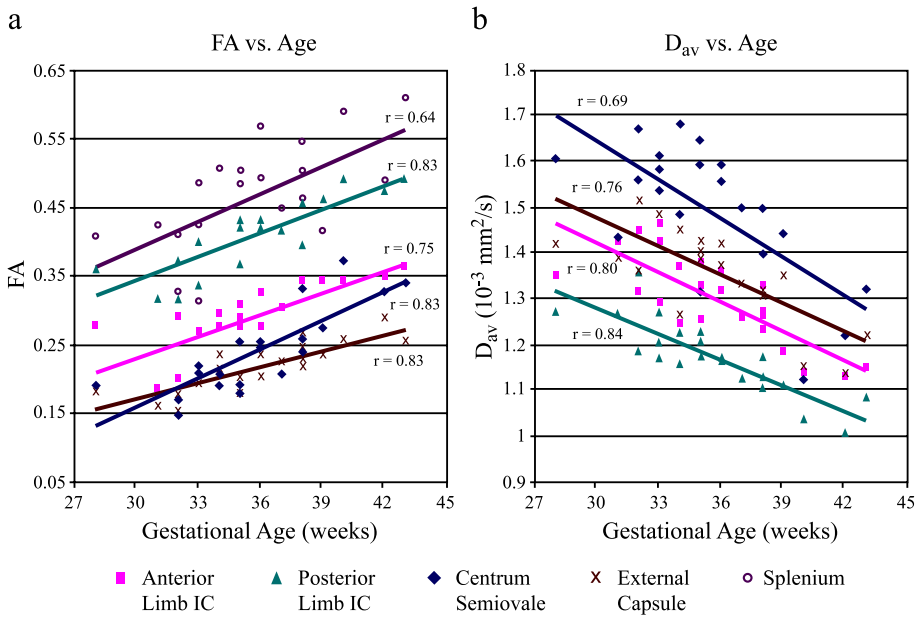

Fig. 3. Comparison of changes in FA (a) and D_{av} (b) with gestational age for the low centrum semiovale and other structures. D_{av} values and variations with age in the splenium were not significantly different from those measured in the anterior limb of the internal capsule (Tables 1 and 2) and therefore D_{av} values in the splenium are not represented on the plot (b) for visual clarity.

Maturational changes

Significant temporal changes were observed in white matter DTI values, and the majority of the structures exhibited similar trends with age ($\downarrow D_{av}$, $\uparrow$ FA, $\downarrow\lambda_2$, $\downarrow\lambda_3$). The major eigenvalue (λ_1) did not change substantially in most structures, but several tracts (of the centrum semiovale, external/extreme capsule, and internal capsule) showed modest negative correlations with age ($\downarrow\lambda_1$). Fig. 3 illustrates the decrease in D_{av} and increase in FA observed with increasing gestational age for all 14 infants. These changes in both D_{av} and FA reflect the changes in the major and minor eigenvalues. For the subjects in this study, large maturational decreases were observed in the two minor eigenvalues (λ_2, λ_3), while the major eigenvalue (λ_1) showed less change with age, especially in those white matter structures with the highest anisotropy. The age dependence of the three eigenvalues is illustrated in Fig. 4 for four representative white matter structures.

Calculations of maturational *rates* were made within the eight subjects studied serially, and the changes in DTI parameters with increasing age are given in Table 3. While most of the white matter structures exhibited significant weekly increases in FA, the weekly D_{av} decreases were smaller and were statistically significant in only six of the regions measured. The maturational rates observed were greatest for FA (ranging from + 2.6% to + 9.13% per week GA), followed by the minor eigenvalues λ_3 (−2.0% to −4.57% per week) and λ_2 (−1.57% to −3.54% per week). Significant maturational rates in D_{av} ranged from −1.06% to −2.88% per week GA. Changes in the maximum eigenvalue, λ_1, were minimal and were statistically significant in only two of the association tracts (ILF and external/extreme capsule) and the subcortical projection pathway of the high centrum semiovale.

Although our sample size was small, we found significant differences in maturation rate (based on increasing FA) between the low centrum semiovale and most other structures (except for the high centrum semiovale and anterior limb of the internal capsule). This particular structure exhibited some of the lowest anisotropy values at younger gestational ages and was found to experience the greatest change with increasing age, with a median rate of increase in FA of 9.13% per week GA.

While the genu and splenium of the corpus callosum were highly anisotropic (the highest FA values of all structures measured) and easily visualized on the anisotropy maps, the measurements with age were also highly variable. In particular for the genu, the FA values appeared to be increasing in some infants and decreasing in others with age. Consequently, no statistically significant maturational trends of the genu of the corpus callosum were identified for any of the DTI parameters.

Discussion

This study utilizing a specialized MR compatible incubator and coil illustrates that even small association pathways and subcortical projection tracts can be successfully visualized and quantitatively characterized in premature neonatal brains using DTI before any detectable myelination on conventional MR imaging or histology. Previous studies of neurologic MR imaging of preterm neonates were performed using standard commercial RF receiver coils (Arzoumanian et al., 2003; Huppi et al., 1998; Miller et al., 2002; Neil et al., 1998) and were hindered by the low sensitivity of these large coils with respect to small infant head sizes, resulting in relatively low SNR and spatial resolution. As a result, prior DTI studies of premature neonates have reported only regional measurements in subcortical white matter (e.g., frontal and parietal regions), with tract-specific measurements limited to only a few large deep projection and commissural pathways, including the internal capsule and corpus callosum (Arzoumanian

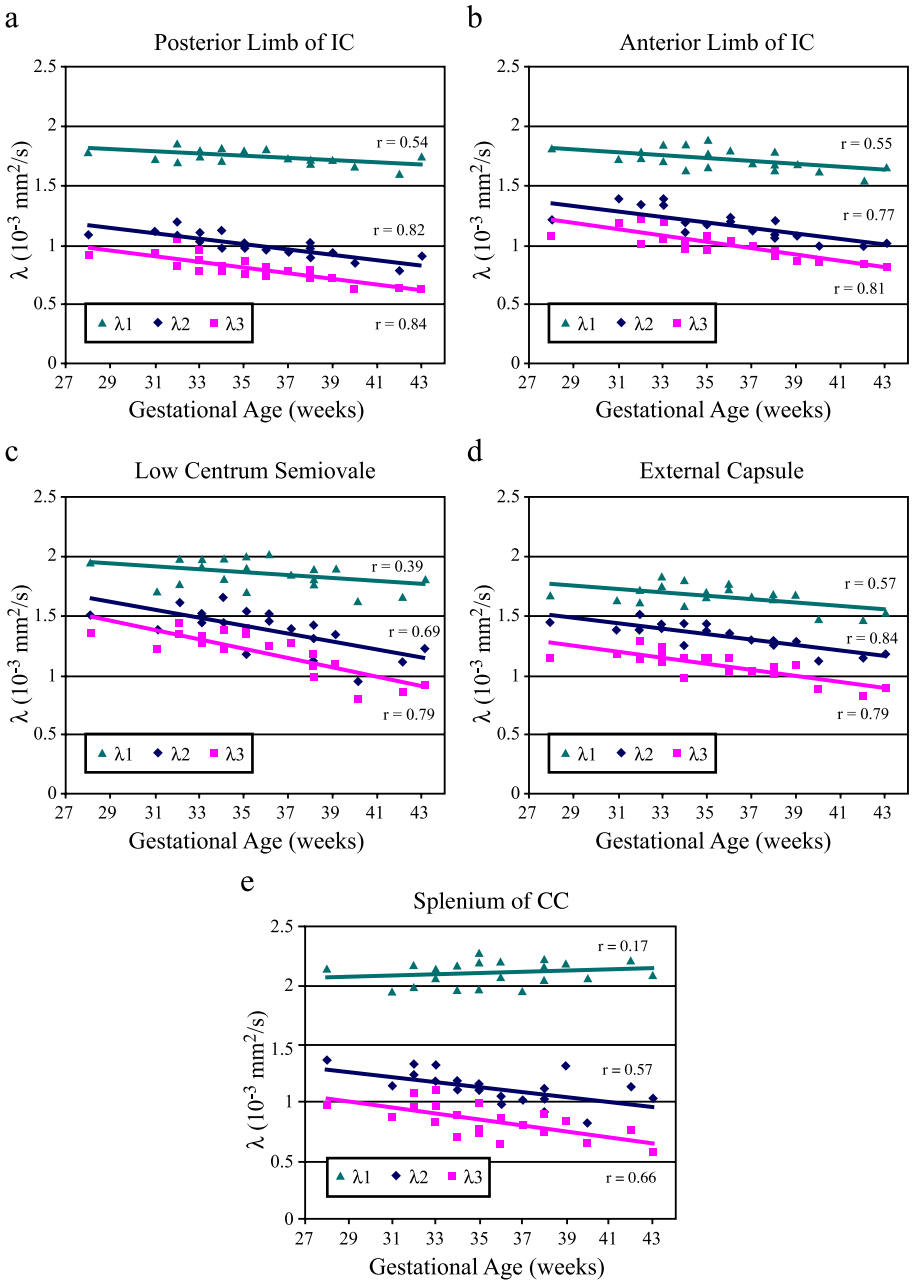

Fig. 4. Comparison of changes in the three diffusion tensor eigenvalues in the posterior limb (a) and anterior limb (b) of the internal capsule, low centrum semiovale (c), external capsule (d), and splenium of the corpus callosum (e). More dramatic maturational changes were observed in the minor eigenvalues, λ_2 and λ_3, than the major eigenvalue, λ_1, especially in high anisotropy commissural white matter (splenium of corpus callosum) and deep projection white matter (internal capsule) compared to low anisotropy association white matter (external capsule) and subcortical projection white matter (low centrum semiovale).

et al., 2003; Huppi et al., 1998; Miller et al., 2002; Neil et al., 1998).

Improvements in DTI imaging and processing

To improve the SNR and spatial resolution for imaging tiny infants, a novel imaging system incorporating both an MR-compatible incubator and specialized high-sensitivity neonatal head coil was developed (Dumoulin et al., 2002). In addition to improvements in the overall image quality obtained, the new system facilitates the imaging of sick or very premature infants by improving the logistics of the transportation and scanning processes and providing a well-monitored, quiet, and temperature-controlled environment during imaging.

Further imaging improvements were obtained by utilizing a single-shot, multi-repetition EPI acquisition, and incorporating a warping image registration algorithm in post-processing to minimize artifacts. Use of the directionally encoded color anisotropy maps greatly facilitated identification of the small white matter tracts. Primary eigenvector maps can provide the same directional information, but must be scaled up substantially for interpretation (Huppi et al., 1998; McKinstry et al., 2002) and can be tedious to

Table 3
Change in DTI parameters (change in value and percent change) per week increase in gestational age

Structure	Diffusion parameter											
	FA		RA		D_{av}		λ_1		λ_2		λ_3	
	Δ	Δ (%)	Δ	Δ (%)	Δ	Δ (%)	Δ	Δ (%)	Δ	Δ (%)	Δ	Δ (%)
	P		P		P		P		P		P	
CC splenium	**0.012**	**2.76**	**0.012**	**3.25**	**−0.026**	**−1.84**	−0.011	−0.50	**−0.040**	**−3.06**	**−0.033**	**−3.33**
	0.01		***0.01***		***0.02***		*0.31*		***0.01***		***0.02***	
CC genu	0.008	1.98	0.008	2.22	−0.010	−0.70	0.002	0.09	−0.005	−0.39	−0.017	−1.84
	0.46		*0.38*		*0.55*		*1.00*		*0.74*		*0.95*	
CC body	**0.010**	**3.37**	**0.009**	***3.71***	−0.025	−1.58	−0.009	−0.44	−0.041	−2.83	−0.022	−1.84
	0.02		***0.02***		*0.20*		*0.55*		*0.15*		*0.06*	
Posterior limb of IC	**0.010**	2.60	**0.010**	**2.97**	**−0.012**	**−1.06**	−0.001	−0.06	**−0.024**	**−2.40**	**−0.021**	**−2.71**
	0.01		***0.01***		***0.01***		*0.74*		***0.01***		***0.01***	
Cerebral peduncle	**0.010**	**3.05**	**0.009**	**3.30**	0.025	0.02	0.021	1.24	−0.011	−1.01	−0.014	−1.87
	0.02		***0.02***		*0.58*		*1.00*		*0.69*		*0.11*	
Anterior limb of IC	**0.011**	**4.03**	**0.010**	**4.38**	**−0.015**	**−1.16**	−0.004	−0.26	**−0.019**	**−1.62**	−0.016	−1.61
	0.01		***0.01***		***0.02***		*0.55*		***0.02***		*0.06*	
Optic radiation	**0.007**	**3.24**	**0.006**	**3.40**	−0.016	−1.16	0.002	0.10	−0.011	−0.78	−0.023	−1.89
	0.01		***0.01***		*0.11*		*0.84*		*0.15*		*0.08*	
Low cent semiovale	**0.018**	**9.13**	**0.016**	**9.57**	**−0.046**	**−2.88**	−0.022	−1.17	**−0.054**	**−3.54**	**−0.056**	**−4.57**
	0.01		***0.01***		***0.02***		*0.31*		***0.02***		***0.01***	
High cent semiovale	**0.007**	**4.36**	**0.006**	**4.48**	**−0.033**	**−1.98**	**−0.019**	**−0.94**	**−0.034**	**−2.05**	**−0.043**	**−2.98**
	0.02		***0.02***		***0.02***		*0.02*		***0.01***		***0.02***	
Cingulum	**0.006**	**2.48**	**0.005**	**2.61**	−0.007	−0.51	0.006	0.29	−0.011	−0.73	**−0.020**	**−1.80**
	0.03		***0.03***		*0.30*		*0.47*		*0.47*		***0.03***	
Inferior LF	0.001	0.51	0.001	0.67	−0.014	−1.17	**−0.016**	**−0.92**	−0.016	−1.20	−0.011	−1.04
	0.47		0.47		*0.08*		*0.03*		*0.30*		*0.16*	
External capsule	**0.006**	**2.90**	**0.006**	**3.03**	**−0.022**	**−1.60**	**−0.017**	**−1.04**	**−0.021**	**−1.57**	**−0.023**	**−2.00**
	0.01		***0.01***		***0.02***		***0.04***		***0.01***		***0.02***	

Data are presented as median change in value, Δ, and percent change per week gestational age, with corresponding *P* values from Wilcoxon signed rank test in italics. Change (Δ) in D_{av}, λ_1, λ_2, λ_3 in units ($\times 10^{-3}$ mm^2/s) per week. Bold represents significant weekly change ($P < 0.05$) based on the signed rank test. Abbreviations: CC = corpus callosum, IC = internal capsule, LF = longitudinal fasciculus.

use for visualization and measurements. Also, white matter fibers having a strong through-plane directional component are poorly represented by primary eigenvector maps. The new DTI acquisition and visualization methods in this study enabled us to image smaller tracts than previously possible and allowed measurements to be made within several association tracts and subcortical projection tracts not previously reported in neonates by MR, including the cingulum, external capsule, centrum semiovale, optic radiations, and inferior longitudinal fasciculus.

Our white matter measurements show systematically lower D_{av} and higher anisotropy values than prior studies of premature newborns (Huppi et al., 1998; Neil et al., 1998). This is due to the superior spatial resolution and more targeted ROI placement within tracts of interest in this investigation, which greatly reduces partial volume averaging with surrounding regions of the brain. The imaging voxel volume for this study was 5.9 mm^3, in comparison with voxel sizes for earlier DTI studies of 11.3 mm^3 (Neil et al., 1998) and 27.6 mm^3 (Huppi et al., 1998). Through these reductions in partial volume averaging, it is predictable that our tract-specific D_{av} values should be lower and our anisotropy measurements higher than prior studies, by minimizing contributions from surrounding less mature and less compact white matter, as well as CSF, both of which have higher D_{av} and lower anisotropy values. Partial volume effects may additionally reduce anisotropy values by including adjacent pathways with different fiber orientations than the tract of interest.

Maturational differences and rates

Significant differences in DTI parameters were observed between white matter pathways. In general, FA was highest in commissural tracts, followed by deep projection tracts, and lowest in subcortical projection and association tracts. This is the same hierarchy of anisotropy found in the fully myelinated white matter tracts of adult volunteers (Shimony et al., 1999), indicating that this hierarchy is already established in the unmyelinated white matter of the preterm brain. Commissural and deep projection white matter tracts are compact bundles of mostly parallel fibers. The high λ_1 values found in the corpus callosum, exceeding 2.0×10^{-3} mm^2/s (Tables 1 and 2, Fig. 4), indicate that fibers in this commissural tract have a high degree of coherent parallel organization, with few barriers to diffusion along the fiber orientation. This explains the high FA of these commissural pathways, despite that fact that the corpus callosum is completely unmyelinated in the preterm newborn (Barkovich, 2000; Kinney et al., 1988, 1994). However, in the more subcortical portions of projection pathways, and along association pathways, there may be divergence of fibers as well as intersections with crossing fibers from other white matter tracts. Moreover, subcortical projection and association tracts mature and myelinate later and more slowly than commissural and deep projection pathways (Barkovich, 2000; Kinney et al., 1988, 1994). These are all factors that can account for the lower

anisotropy of subcortical projection and association pathways in the developing human brain, relative to commissural and deep projection tracts.

The most sensitive DTI measure for detecting differences between tracts was diffusion anisotropy, primarily because the maturational changes in white matter anisotropy were larger than those in any individual eigenvalue, or in the mean of the three eigenvalues, D_{av}, which was the least sensitive measure. Furthermore, it was proposed that the expansive nonlinearity at low anisotropy values provided by the FA index may better distinguish small differences in anisotropy in the neonatal brain than would the more linear RA index (Ulug and van Zijl, 1999). Indeed, this was true for our study of premature newborns where FA values ranged from 0.14 to 0.61 (mean, 0.31). FA performed as well or better than RA for all pairwise comparisons of structures, distinguishing between all the same pairs of regions as RA plus two additional pairs. As expected, the white matter structures that were separable only by FA, and not RA, were on the lower end of the anisotropy scale (anterior limb of internal capsule versus cingulum and high centrum semiovale versus inferior longitudinal fasciculus), with mean FA values ranging from 0.20 to 0.29. The higher sensitivity of FA for low anisotropy structures suggests that FA is preferable to RA for the quantitative characterization of white matter tracts in premature neonates. In addition, a recent study validated that FA has superior noise characteristics relative to RA, and that FA images have higher SNR than RA for anisotropic regions, further supporting the use of FA over RA (Hasan et al., 2004).

The lowest D_{av} values were found in the pyramidal tract at the posterior limb of the internal capsule and at the cerebral peduncle (Tables 1 and 2). Of the 12 white matter structures in this study, these are the only two that begin to myelinate during preterm gestation; the remaining 10 structures remain unmyelinated in the premature brain (Barkovich, 2000; Kinney et al., 1988, 1994). During childhood brain maturation, myelination has been shown to preferentially reduce the minor eigenvalues λ_2 and λ_3, by hindering diffusion in the plane orthogonal to the fiber orientation (Mukherjee et al., 2002). We extend this finding to the preterm human brain, by showing that the myelinating tracts of the cerebral peduncle and posterior limb of the internal capsule have lower λ_2 and λ_3 values than the other 10 unmyelinated white matter structures. D_{av}, the mean of the three eigenvalues, is therefore also lower in these two myelinating structures. The preferential reduction of the two minor eigenvalues compared to the major eigenvalue in these two structures also results in relatively high FA, consistent with the known increases in anisotropy associated with myelination in neonates (Huppi et al., 1998; Miller et al., 2002; Neil et al., 1998) and children (McGraw et al., 2002; Mukherjee et al., 2001, 2002). Although unmyelinated, the highly collimated commissural white matter of the genu and splenium of the corpus callosum still demonstrated higher FA than the myelinating deep projection tracts at the cerebral peduncle and the posterior limb of the internal capsule, largely due to greater values of the major eigenvalue λ_1 (Fig. 4). This disparity persists throughout childhood (Mukherjee et al., 2002) and into adulthood (Shimony et al., 1999), when all of these fiber tracts are fully myelinated.

Decreasing D_{av} and increasing anisotropy with increasing gestational age was identified in the developing white matter of premature neonates, similar to previous findings (Huppi et al., 1998; Miller et al., 2002). We extend these prior observations to show that, across serial measurements, these reductions in D_{av} and increases in FA are due primarily to decreases in the two minor eigenvalues, λ_2 and λ_3 (Table 3, Fig. 4). This trend of preferential reduction of the two minor eigenvalues with progressive white matter maturation has been shown to continue during childhood brain maturation (Mukherjee et al., 2002). Interestingly, we found no discontinuity in the maturational trends of the DTI parameters coincident with the transition from premyelination to myelination, which occurs at approximately 36 weeks GA in the posterior limb of the internal capsule and even earlier in the cerebral peduncle (Barkovich, 2000; Kinney et al., 1988, 1994). The onset of myelination, easily visible on conventional T1-weighted and T2-weighted imaging (Barkovich et al., 1988), was therefore not readily distinguished based on the DTI parameters, which depicted a smoother, more continuous maturational process. We do not yet have sufficient serial data covering the appropriate age ranges for this particular stage of development, so further investigation is necessary to more sensitively assess whether distinct stages of the premyelination and myelination process can be discerned from the quantitative trends of DTI parameters.

In the serially followed preterm neonates, we found maturational changes over the age range of 28–43 weeks GA to be more dramatic in the subcortical projection pathways of the centrum semiovale, with steeper declines in D_{av} and increases in FA, than in the deep portions of these same projection tracts at the internal capsule and cerebral peduncle (Table 3). Continued faster growth of anisotropy in more peripheral subcortical white matter compared to deep central white matter has been documented by McGraw et al. (2002) in infants and children during the first six years of life.

Greater variation in DTI values was observed in the corpus callosum than in other white matter tracts. In serial studies, the genu of the corpus callosum in particular exhibited highly variable age-related changes across different individuals for both D_{av} and FA. Variability in corpus callosum measures has been reported by others as well, and the cause is thought to be due to increased noise from CSF pulsatile motion artifacts in regions bordering the ventricles (Mukherjee et al., 2001, 2002; Pfefferbaum et al., 2000). Moreover, there may be less maturational change during preterm development in the genu of the corpus callosum than in other white matter structures, since the frontal lobes are known to mature later and more slowly than other brain regions (Barkovich, 2000; Kinney et al., 1988, 1994).

The fact that the water content of the brain decreases with increasing age in neonates should be considered when interpreting brain diffusion changes with age. This topic has been explored in detail in prior DTI studies of newborns, infants, and children (Mukherjee et al., 2002; Neil et al., 1998). Our results are consistent with these prior investigations in that some of the decrease in D_{av} can be attributed to decreasing brain water content, but the percent decrease in D_{av} is much greater than the percent decline in brain water content over the same age range (Dobbing and Sands, 1973). This indicates that decreases in D_{av} reflect more than just tissue water loss. Also, one would expect that a decrease in brain water content would cause reduced water motion proportional along all axes, which should not produce a change in diffusion anisotropy. The increases in anisotropy we measured with age primarily reflected decreases in the minor eigenvalues (λ_2 and λ_3), and little change in the major eigenvalue (λ_1). This suggests that the changes in anisotropy are not simply explained by changes in brain water content, and more likely reflect microstructural changes of premyelination and myelination, causing

increased hindrance to water diffusion perpendicular to the direction of axonal fibers.

Conclusions

Our new DTI acquisition and analysis methods improved detection and quantitation of unmyelinated white matter tracts in preterm newborns over prior studies. These improvements enabled tract-specific characterization of maturing white matter, including several association tracts and subcortical projection tracts not previously investigated in neonates by MR imaging. Significant differences in DTI parameters were observed between white matter pathways, with earlier maturing commissural tracts of the corpus callosum and deep projection tracts of the cerebral peduncle and internal capsule exhibiting lower D_{av} and higher FA than later maturing subcortical projection and association pathways. The same hierarchy of anisotropy has been shown in fully myelinated white matter tracts of adult volunteers (Shimony et al., 1999), indicating that this hierarchy is already established in the unmyelinated white matter of the preterm brain. The maturational changes observed in serial measurements of the same infants included reductions in D_{av} and increases in FA with age, which resulted primarily from decreases in the two minor diffusion eigenvalues, λ_2 and λ_3. These maturational changes were more pronounced in the subcortical projection pathways of the centrum semiovale than in the deep portions of these same projection tracts at the internal capsule and cerebral peduncle.

The advent of 3D diffusion tensor fiber tractography (Basser et al., 2000; Conturo et al., 1999; Mori et al., 1999; Poupon et al., 2000) may further improve tract-specific quantitation of white matter maturation by enabling the measurement of DTI parameters along the entire 3D trajectory of an axonal pathway, rather than at only discrete locations within the tract. Improved quantitative evaluation of white matter development in premature newborns should enable earlier, more sensitive detection of white matter injury of prematurity and provide a better understanding as to how white matter injury of prematurity affects subsequent brain development. This prognostic information may affect clinical decisions regarding aggressiveness of care, including enrollment in experimental trials of neuroprotective agents or initiation of rehabilitation therapy.

Acknowledgments

The authors wish to thank Srivathsa Veeraraghavan, B.S. for assistance in acquiring and processing the MR data, and the neonatal nurses of the Pediatric Clinical Research Center, in particular Nancy Newton, R.N., without whose enthusiastic collaboration, this study of premature infants would not have been possible. We also acknowledge grant funding from the NIH (RO1 NS40117, R21 NS40382, RR01271, and P50 NS35902).

References

Arzoumanian, Y., Mirmiran, M., Barnes, P.D., Woolley, K., Ariagno, R.L., Moseley, M.E., Fleisher, B.E., Atlas, S.W., 2003. Diffusion tensor brain imaging findings at term-equivalent age may predict neurologic abnormalities in low birth weight preterm infants. AJNR Am. J. Neuroradiol. 24 (8), 1646–1653.

Barkovich, A.J., 2000. Concepts of myelin and myelination in neuroradiology. AJNR Am. J. Neuroradiol. 21 (6), 1099–1109.

Barkovich, A.J., Kjos, B.O., Jackson Jr., D.E., Norman, D. 1988. Normal maturation of the neonatal and infant brain: MR imaging at 1.5 T. Radiology 166 (1 Pt 1), 173–180.

Basser, P.J., Pierpaoli, C., 1996. Microstructural and physiological features of tissues elucidated by quantitative-diffusion-tensor MRI. J. Magn. Reson., B 111 (3), 209–219.

Basser, P.J., Pajevic, S., Pierpaoli, C., Duda, J., Aldroubi, A., 2000. In vivo fiber tractography using DT-MRI data. Magn. Reson. Med. 44 (4), 625–632.

Bhutta, A.T., Cleves, M.A., Casey, P.H., Cradock, M.M., Anand, K.J., 2002. Cognitive and behavioral outcomes of school-aged children who were born preterm: a meta-analysis. JAMA 288 (6), 728–737.

Boujraf, S., Luypaert, R., Shabana, W., De Meirleir, L., Sourbron, S., Osteaux, M., 2002. Study of pediatric brain development using magnetic resonance imaging of anisotropic diffusion. Magn. Reson. Imaging 20 (4), 327–336.

Conturo, T.E., Lori, N.F., Cull, T.S., Akbudak, E., Snyder, A.Z., Shimony, J.S., McKinstry, R.C., Burton, H., Raichle, M.E., 1999. Tracking neuronal fiber pathways in the living human brain. Proc. Natl. Acad. Sci. U. S. A. 96 (18), 10422–10427.

Dobbing, J., Sands, J., 1973. Quantitative growth and development of human brain. Arch. Dis. Child. 48 (10), 757–767.

Dumoulin, C.L., Rohling, K.W., Piel, J.E., Rossi, C.J., Giaquinto, R.O., Watkins, R.D., Vigneron, D.B., Barkovich, A.J., Newton, N., 2002. Magnetic resonance imaging compatible neonate incubator. Magn. Reson. Engineering 15, 117–128.

Fombonne, E., 2003. Epidemiological surveys of autism and other pervasive developmental disorders: an update. J. Autism Dev. Disord. 33 (4), 365–382.

Hack, M., Flannery, D.J., Schluchter, M., Cartar, L., Borawski, E., Klein, N., 2002. Outcomes in young adulthood for very-low-birth-weight infants. N. Engl. J. Med. 346 (3), 149–157.

Hasan, K.M., Alexander, A.L., Narayana, P.A., 2004. Does fractional anisotropy have better noise immunity characteristics than relative anisotropy in diffusion tensor MRI? An analytical approach. Magn. Reson. Med. 51 (2), 413–417.

Hochberg, Y., Tamhane, A.C., 1987. Multiple Comparison Procedures. Wiley, New York, pp. 85–101.

Huppi, P.S., Maier, S.E., Peled, S., Zientara, G.P., Barnes, P.D., Jolesz, F.A., Volpe, J.J., 1998. Microstructural development of human newborn cerebral white matter assessed in vivo by diffusion tensor magnetic resonance imaging. Pediatr. Res. 44 (4), 584–590.

Huppi, P.S., Murphy, B., Maier, S.E., Zientara, G.P., Inder, T.E., Barnes, P.D., Kikinis, R., Jolesz, F.A., Volpe, J.J., 2001. Microstructural brain development after perinatal cerebral white matter injury assessed by diffusion tensor magnetic resonance imaging. Pediatrics 107 (3), 455–460.

Inder, T.E., Anderson, N.J., Spencer, C., Wells, S., Volpe, J.J., 2003. White matter injury in the premature infant: a comparison between serial cranial sonographic and MR findings at term. AJNR Am. J. Neuroradiol. 24 (5), 805–809.

Kinney, H.C., Brody, B.A., Kloman, A.S., Gilles, F.H., 1988. Sequence of central nervous system myelination in human infancy: II. Patterns of myelination in autopsied infants. J. Neuropathol. Exp. Neurol. 47 (3), 217–234.

Kinney, H.C., Karthigasan, J., Borenshteyn, N.I., Flax, J.D., Kirschner, D.A., 1994. Myelination in the developing human brain: biochemical correlates. Neurochem. Res. 19 (8), 983–996.

Laird, N.M., Ware, J.H., 1982. Random-effects models for longitudinal data. Biometrics 38 (4), 963–974.

Maritz, J.S., 1985. Models and the use of signed rank tests. Stat. Med. 4 (2), 145–153.

Martin, J.A., Hamilton, B.E., Ventura, S.J., Menacker, F., Park, M.M., 2002. Births: final data for 2000. Natl. Vital Stat. Rep. 50 (5), 1–101.

McGraw, P., Liang, L., Provenzale, J.M., 2002. Evaluation of normal age-related changes in anisotropy during infancy and childhood as shown by diffusion tensor imaging. AJR Am. J. Roentgenol. 179 (6), 1515–1522.

McKinstry, R.C., Mathur, A., Miller, J.H., Ozcan, A., Snyder, A.Z., Schefft, G.L., Almli, C.R., Shiran, S.I., Conturo, T.E., Neil, J.J., 2002. Radial organization of developing preterm human cerebral cortex revealed by non-invasive water diffusion anisotropy MRI. Cereb. Cortex 12 (12), 1237–1243.

Ment, L.R., Bada, H.S., Barnes, P., Grant, P.E., Hirtz, D., Papile, L.A., Pinto-Martin, J., Rivkin, M., Slovis, T.L., 2002. Practice parameter: neuroimaging of the neonate: report of the Quality Standards Subcommittee of the American Academy of Neurology and the Practice Committee of the Child Neurology Society. Neurology 58 (12), 1726–1738.

Miller, S.P., Vigneron, D.B., Henry, R.G., Bohland, M.A., Ceppi-Cozzio, C., Hoffman, C., Newton, N., Partridge, J.C., Ferriero, D.M., Barkovich, A.J., 2002. Serial quantitative diffusion tensor MRI of the premature brain: development in newborns with and without injury. J. Magn. Reson. Imaging 16 (6), 621–632.

Miller, S.P., Cozzio, C.C., Goldstein, R.B., Ferriero, D.M., Partridge, J.C., Vigneron, D.B., Barkovich, A.J., 2003. Comparing the diagnosis of white matter injury in premature newborns with serial MR imaging and transfontanel ultrasonography findings. AJNR Am. J. Neuroradiol. 24 (8), 1661–1669.

Mori, S., Crain, B.J., Chacko, V.P., van Zijl, P.C., 1999. Three-dimensional tracking of axonal projections in the brain by magnetic resonance imaging. Ann. Neurol. 45 (2), 265–269.

Mukherjee, P., Miller, J.H., Shimony, J.S., Conturo, T.E., Lee, B.C., Almli, C.R., McKinstry, R.C., 2001. Normal brain maturation during childhood: developmental trends characterized with diffusion-tensor MR imaging. Radiology 221 (2), 349–358.

Mukherjee, P., Miller, J.H., Shimony, J.S., Philip, J.V., Nehra, D., Snyder, A.Z., Conturo, T.E., Neil, J.J., McKinstry, R.C., 2002. Diffusion-tensor MR imaging of gray and white matter development during normal human brain maturation. AJNR Am. J. Neuroradiol. 23 (9), 1445–1456.

Neil, J.J., Shiran, S.I., McKinstry, R.C., Schefft, G.L., Snyder, A.Z., Almli, C.R., Akbudak, E., Aronovitz, J.A., Miller, J.P., Lee, B.C., Conturo, T.E., 1998. Normal brain in human newborns: apparent diffusion coefficient and diffusion anisotropy measured by using diffusion tensor MR imaging. Radiology 209 (1), 57–66.

Pajevic, S., Pierpaoli, C., 1999. Color schemes to represent the orientation of anisotropic tissues from diffusion tensor data: application to white matter fiber tract mapping in the human brain. Magn. Reson. Med. 42 (3), 526–540.

Pfefferbaum, A., Sullivan, E.V., Hedehus, M., Lim, K.O., Adalsteinsson, E., Moseley, M., 2000. Age-related decline in brain white matter anisotropy measured with spatially corrected echo-planar diffusion tensor imaging. Magn. Reson. Med. 44 (2), 259–268.

Poupon, C., Clark, C.A., Frouin, V., Regis, J., Bloch, I., Le Bihan, D., Mangin, J., 2000. Regularization of diffusion-based direction maps for the tracking of brain white matter fascicles. NeuroImage 12 (2), 184–195.

Prayer, D., Barkovich, A.J., Kirschner, D.A., Prayer, L.M., Roberts, T.P., Kucharczyk, J., Moseley, M.E., 2001. Visualization of nonstructural changes in early white matter development on diffusion-weighted MR images: evidence supporting premyelination anisotropy. AJNR Am. J. Neuroradiol. 22 (8), 1572–1576.

Shimony, J.S., McKinstry, R.C., Akbudak, E., Aronovitz, J.A., Snyder, A.Z., Lori, N.F., Cull, T.S., Conturo, T.E., 1999. Quantitative diffusion-tensor anisotropy brain MR imaging: normative human data and anatomic analysis. Radiology 212 (3), 770–784.

Spencer, T.J., Biederman, J., Wilens, T.E., Faraone, S.V., 2002. Overview and neurobiology of attention-deficit/hyperactivity disorder. J. Clin. Psychiatry 63 (Suppl. 12), 3–9.

Ulug, A.M., van Zijl, P.C., 1999. Orientation-independent diffusion imaging without tensor diagonalization: anisotropy definitions based on physical attributes of the diffusion ellipsoid. J. Magn. Reson. Imaging 9 (6), 804–813.

Volpe, J.J., 2001. Neurology of the Newborn, 4th ed. Saunders, Philadelphia.

Wimberger, D.M., Roberts, T.P., Barkovich, A.J., Prayer, L.M., Moseley, M.E., Kucharczyk, J., 1995. Identification of ''premyelination'' by diffusion-weighted MRI. J. Comput. Assist. Tomogr. 19 (1), 28–33.

Woods, R.P., Grafton, S.T., Holmes, C.J., Cherry, S.R., Mazziotta, J.C., 1998a. Automated image registration: I. General methods and intrasubject, intramodality validation. J. Comput. Assist. Tomogr. 22 (1), 139–152.

Woods, R.P., Grafton, S.T., Watson, J.D., Sicotte, N.L., Mazziotta, J.C., 1998b. Automated image registration: II. Intersubject validation of linear and nonlinear models. J. Comput. Assist. Tomogr. 22 (1), 153–165.

Wood, N.S., Marlow, N., Costeloe, K., Gibson, A.T., Wilkinson, A.R., 2000. Neurologic and developmental disability after extremely preterm birth. EPICure Study Group. N. Engl. J. Med. 343 (6), 378–384.